Nuclear Science and Techniques (2024) 35:68
https://doi.org/10.1007/s41365-024-01428-y

Plutonium utilization in a small modular molten-salt reactor based on a batch fuel reprocessing scheme

Xue-Chao Zhao[1,2] · Rui Yan[1,2,3] · Gui-Feng Zhu[1,2,3] · Ya-Fen Liu[1,2] · Jian Guo[1,2,3] · Xiang-Zhou Cai[1,2,3] · Yang Zou[1,2,3]

Received: 30 November 2022 / Revised: 3 November 2023 / Accepted: 11 November 2023 / Published online: 9 May 2024

Abstract

A molten salt reactor (MSR) has outstanding features considering the application of thorium fuel, inherent safety, sustainability, and resistance to proliferation. However, fissile material ^{233}U is significantly rare at the current stage, thus it is difficult for MSR to achieve a pure thorium-uranium fuel cycle. Therefore, using plutonium or enriched uranium as the initial fuel for MSR is more practical. In this study, we aim to verify the feasibility of a small modular MSR that utilizes plutonium as the starting fuel (SM-MSR-Pu), and highlight its advantages and disadvantages. First, the structural design and fuel management scheme of the SM-MSR-Pu were presented. Second, the neutronic characteristics, such as the graphite-irradiation lifetime, burn-up performance, and coefficient of temperature reactivity were calculated to analyze the physical characteristics of the SM-MSR-Pu. The results indicate that plutonium is a feasible and advantageous starting fuel for a SM-MSR; however, there are certain shortcomings that need to be solved. In a 250 MWth SM-MSR-Pu, approximately 288.64 kg ^{233}U of plutonium with a purity of greater than 90% is produced while 978.00 kg is burned every ten years. The temperature reactivity coefficient decreases from −4.0 to −6.5 pcm K^{-1} over the 50-year operating time, which ensures a long-term safe operation. However, the amount of plutonium and accumulation of minor actinides (MAs) would increase as the burn-up time increases, and the annual production and purity of ^{233}U will decrease. To achieve an optimal burn-up performance, setting the entire operation time to 30 years is advisable. Regardless, more than 3600 kg of plutonium eventually accumulate in the core. Further research is required to effectively utilize this accumulated plutonium.

Keywords Molten salt fuel · Plutonium utilization · ^{233}U · TRUs mole fraction · Temperature feedback coefficient

1 Introduction

Molten salt reactors (MSRs) are an alternative for the fourth generation of nuclear systems owing to their remarkable performances in thorium resource utilization, inherent safety, sustainability, and non-proliferation [1–3]. A molten salt reactor is also the only type of reactor that uses liquid fuel, which can achieve on-line fuel feeding and online processing fission products (FPs), and is an ideal reactor for thorium resource utilization [4–8]. Increasing countries are engaged in studying the thorium-based MSR (TMSR), reporting several conceptual designs [9–11]. In addition to the mainstream fluoride salt reactor, certain reactors, such as the subcritical MSR, chloride MSR, and micro MSR, have also been studied to achieve certain specific goals [12–15]. A TMSR, which utilizes ^{233}U as the starting fuel, can achieve a pure thorium-uranium fuel

This work was supported by the Chinese TMSR Strategic Pioneer Science and Technology Project (No.XDA02010000), Chinese Academy of Sciences Talent Introduction Youth Program (No. SINAP-YCJH-202303), Chinese Academy of Sciences Special Research Assistant Funding Project and Shanghai Pilot Program for Basic Research - Chinese Academy of Science, Shanghai Branch(JCYJ-SHFY-2021-003).

✉ Xue-Chao Zhao
zhaoxuechao@sinap.ac.cn

✉ Yang Zou
zouyang@sinap.ac.cn

[1] Shanghai Institute of Applied Physics, Chinese Academy of Sciences, Shanghai 201800, China

[2] CAS Innovative Academies in TMSR Energy System, Chinese Academy of Sciences, Shanghai 201800, China

[3] University of Chinese Academy of Sciences, Beijing 100049, China

cycle and minimum accumulation of radioactive nuclear waste. However, owing to the difficulty in quickly establishing a thorium-uranium cycle in a TMSR without a large supply of ^{233}U fuel, the earliest molten salt reactors used other fuels for starting, such as low-enrichment uranium (LEU) or plutonium extracted from the pressurized water reactor (PWR)-spent fuel. Although traditional enriched uranium can be used as the starting fuel for the transition to a thorium-uranium fuel cycle, a higher ^{235}U enrichment degree is required, which is significantly challenging for nuclear non-proliferation. An advantage of plutonium as a start-up fuel over enriched uranium is that ^{233}U is nearly the only uranium isotope mixed in molten salts and is relatively easy to separate by volatilizing fluoride. The accumulation of plutonium in PWRs is gaining increasing attention, thus research regarding the burning of plutonium in a molten salt reactor or driving the thorium and uranium proliferation with plutonium is also increasing [16, 17]. Several studies regarding the molten salt fast reactor (MSFR) in France demonstrate that it can produce ^{233}U more efficiently by burning plutonium under a fast spectrum. In addition, studies have shown that burning plutonium and breeding ^{233}U in a MSR with a thermal neutron spectrum can achieve an extremely high plutonium-utilization efficiency [18].

Small modular reactors have recently gained significant interest owing to their simplified design and construction, flexibility, and passive safety [19–21]. Benefiting from various fuel processing schemes, a small-scale MSR can also achieve effective utilization of thorium resources. The thorium-uranium breeding mode with on-line fuel processing can theoretically achieve the most thorough thorium fuel conversion and is the ideal means for the MSR thorium fuel cycle. However, this fuel utilization method is nearly impossible in the short-term, which is restricted by on-line dry-processing technology. Therefore, the off-line batch reprocessing fuel management scheme is considered to be a preferable transition strategy for MSR in the near future. The Fuji-U3 concept developed in Japan adopts a fuel batch-processing scheme, in which the graphite component is replaced and the off-line processing of fuel is performed every 7.5 years [22]. The helium bubble system can continuously remove gaseous and insoluble fission products (FPs), and fluorination volatilization technology can separate most other FPs from actinide fuel [23]. An excellent Th-^{233}U fuel-conversion performance can be achieved in this manner. Another Fuji reactor (Fuji-Pu), which is designed to burn plutonium, can achieve a higher ^{233}U production than other FUJI reactors within the same amount of time [24]. The design of a transatomic power molten salt reactor (TAP-MSR) is based on the MSR concept using ZrH as a moderator, which can satisfy an extremely high plutonium utilization efficiency [25]. The relevant research conducted by the Chinese Academy of Sciences (CAS) demonstrates that using plutonium as the starting fissile material in a thermal MSR is highly desirable, which can quickly start the thorium fuel cycle and establish operating characteristics similar to the ^{233}U starting core [26, 27]. Considering a special core design and by optimizing the fuel management scheme, a small modular MSR can efficiently utilize PWR plutonium, thus alleviating the problem of ^{233}U fuel shortage in the thorium uranium cycle.

In this study, we will try to verify the achievability of this small modular MSR, which uses plutonium as the starting fuel, and discuss its advantages and disadvantages. A specific SM-MSR-Pu core structure was designed to achieve the efficient utilization of PWR spent fuel and thorium resources. The structural design and fuel management scheme of the SM-MSR-Pu were presented. Plutonium extracted from the PWR discharge was used as the fissile fuel, and thorium was used as the breeder fuel. The lifetimes of the reactor core and fuel reprocessing cycle were set to 10 years. During the operating life of each generation core, an on-line bubbling system is the only processing scheme used to remove insoluble FPs. Although the low fuel conversion ratio (CR) is insufficient for maintaining the reactivity, a long-term operation can be maintained by the on-line fuel feeding of plutonium to compensate for the neutron loss from the absorption of fission products. The SM-MSR-Pu scheme considers both the off-line post-processing, incineration of plutonium, and production of ^{233}U. It can burn the PWR plutonium to solve the problem of self-sustaining fission fuel in small MSRs. First, the design and fuel management schemes of the SM-MSR-Pu are described in this study. Subsequently, the neutron energy spectrum, neutron spatial distribution, and temperature reactivity coefficient were calculated to analyze the neutron properties, graphite irradiation life, and safety performance. In addition, the production and purity of ^{233}U, consumption and amount of plutonium, as well as the accumulation of minor actinides (MAs) were presented to analyze the fuel burn-up performance of SM-MSR-Pu.

2 General description and optimization

2.1 Schematic model of the SM-MSR-Pu

The SM-MSR-Pu consists of the active region, fuel chambers, radial reflector, axial reflector, control rod system, heat exchanger system, reactor vessel, and other structural parts. The core structure is shown in Fig. 1. The fuel salts of the primary circuit are mostly distributed in the graphite active region, fuel chambers, heat exchanger systems, and pipelines. The height and diameter of the active region are 3.2 m and 3.0 m, respectively. It is composed of 199

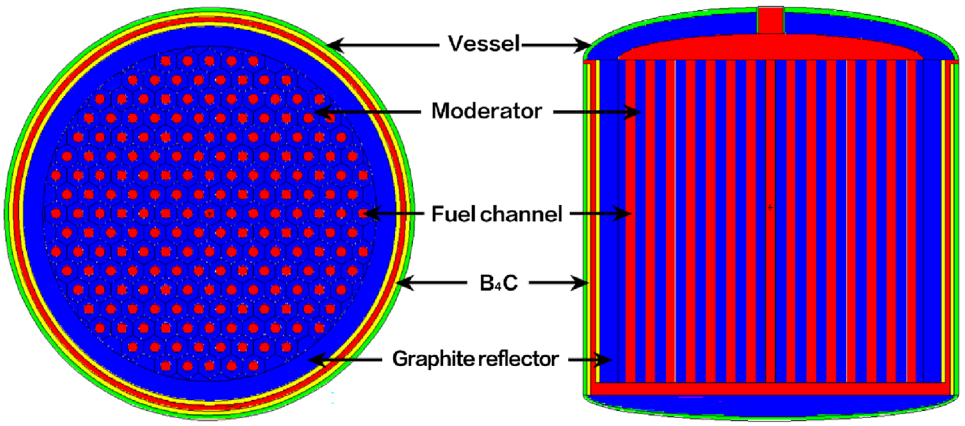

Fig. 1 (Color online) Geometrical description of the SM-MSR-Pu core

graphite hexagonal prism assemblies whose hexagon pitch size is 20 cm. Graphite subassemblies connect the upper and lower via the card slot, and are finally pressed and fixed by the upper and lower support plate. The supporting plate is a honeycomb structure, composed of hastelloy alloy material, 2.0 cm thick, and embedded in the groove of the graphite assembly. It is located on the core container support, which is used to support all the weight of the reactor core.

The graphite reflector is formed by 12 fan-shaped annular graphite tips with an equivalent thickness of 20 cm. A 2.0 cm-thick layer of the B_4C neutron absorber is installed on the outside of the horizontal graphite reflector, primarily to protect the reactor vessel from neutron leakage from the core. Outside the reflector layer, there is a 1.0-cm thick core barrel, which is composed of Hastelloy material to radially fix the graphite tip and form a stable descending ring cavity with the outer container.

Varying from solid fuel assemblies, liquid fuel salts of SM-MSR-Pu also serve as the coolant, circulating in the primary circuit and transferring heat. The designed maximum operating power of the SM-MSR-Pu is 250 MWth, and the average power density of the active zone is 11.0 W/cm^3. The electrical power is 100 MW, which is significantly lower than the standard for small reactors (<300 MWe). The designed power and vessel size satisfy the standards of a small modular reactor. The module of the reactor container meets a variety of land transportation standards. Based on the minimum limit of railways and highways, the diameter of the container body was designed according to the limit of less than 3.88 m. Each component of the reactor adopts a modular design, which can be processed and produced in the factory and transported to the destination for installation via railways or highways. The composition and molar ratio of molten salt are as follows: 70%LiF+17.5%BeF_2+12.5%(ThF_4+PuF_3), and the enrichment of Li-7 is 99.995%. The starting fuel, plutonium, is extracted from the spent fuel of a PWR, which consists of approximately 1.8% ^{238}Pu, 59% ^{239}Pu, 23% ^{240}Pu, 12.2% ^{239}Pu, 4% ^{242}Pu [12]. The brief physical parameters of the core structure are provided in Table 1.

Table 1 Brief physical parameters of SM-MSR-Pu

Key parameter	Value
Maximum thermal power (MWth)	250
Fuel salt	
Fuel composition	LiF- BeF_2- (ThF_4+PuF_3)
Fuel (mol.fraction%)	70 −17.5 −12.5
Starting fuel	Pu + Th
Feed fuel	Pu
Fuel density (g/cm^3)	3.3
Fuel reprocessing cycle (years)	10
Core size	
Diameter (m)	3.54
Height (m)	3.60
Diameter of active region (m)	3.00
Height of active region (m)	3.20
Thickness of reflector (cm)	20
Number of fuel channels	199
Fuel channel radius (cm)	4.70
Graphite subassembly hexagon size (cm)	20
Average temperature(K)	900

The off-line batch fuel-processing scheme is adopted in the SM-MSR-Pu. In other MSR designs for fuel breeding, including the molten-salt breeder reactor (MSBR) and molten-salt fast reactor (MSFR), the fuel conversion ability of MSR can be significantly improved by on-line fuel processing technology. Theoretically, MSRs with a closed fuel cycle can be optimized by utilizing thorium resources, and can be considered one of the best models of the thorium uranium cycle [28, 29]. However, on-line fuel processing is restricted by on-line dry-processing technology, which is difficult to achieve in the short term.

Therefore, off-line processing is considered to be a preferable transition strategy from the once-through fuel scheme to the on-line processing fuel scheme.

The off-line batch processing scheme of SM-MSR-Pu is mainly based on the helium bubbling system and electrochemical separation system, which can achieve reprocessing of the batch fuel and the on-line continuous removal of insoluble FPs. The reprocessing flowchart of the batch mode is shown in Fig. 2. The helium bubble system is an on-line fuel processing module based on the physical separation method of gas and liquid. A special blowing device is used to blow helium gas into the molten salt fuel in the primary circuit. These helium gases simultaneously flow with the fuel in the primary circuit and are finally separated from the fuel using a gas separation device. Through this process, insoluble gases and heavy metals such as H, He, N, O, Ne, Ar, Kr, Nb, Mo, Tc, Ru, Rh, Pd, Ag, Sb, Te, Xe, Rn, and other fission products can be removed from the reactor core; the separation efficiency of this method is significantly high. The extraction time of each bubble-processing cycle was set to 30 s in this study. The electrochemical separation system treats molten salt fuel using electrochemical methods and separates the soluble fission products (such as lanthanides) or secondary actinides that cannot be separated by the bubbling system from the molten salt, and returns the remaining molten salt, including most of the actinides, to the core.

On-line refueling is another fuel management technology applicable to molten salt reactors. On-line refueling can achieve lower excess reactivity and lower initial fuel loading, while reducing certain requirements for the control rod systems. The critical operating state is easier to maintain by coordinating the operation of the control rods and fuel supply modules. In the fuel scheme of SM-MSR-Pu, dry reprocessing technologies such as fluorination and volatilization, reductive extraction, and reduced pressure distillation are used to separate U, Th, transuranic isotopes(TRUs), and FPs. U, Np, and Pu are first extracted by the fluorination reaction and quickly reinjected into the core, whereas FPs and other discarded salts are further processed, encapsulated, and stored underground.

2.2 Calculation tool and methodology

To calculate the burn-up in molten salt reactors with fuel reprocessing, our colleagues developed a customized MSR reprocessing sequence (MSR-RS) [30] that can be applied to the on-line refueling and off-line batch processing for the SM-MSR-Pu. The MSR-RS program is coupled with CSAS6 (criticality analysis module), TRITON (problem-dependent cross section processing module), and ORIGEN-S (depletion and decay calculation module) in the SCALE6.1 program.

The calculation flowchart of the MSR-RS is shown in Fig. 3. After initializing the fuel compositions and core geometry, the TRITON and ORIGEN-S modules are called for neutron transport and depletion calculations, respectively. The specified isotopes set by the user can be reprocessed, and the required fuel will be refueled to maintain the criticality of the reactor. In addition, the CSAS6 module was used to provide a new keff value, a 238-group ENDF/B-VII cross-sectional database was selected, and 388 nuclides were tracked in trace quantities. The nuclide neutron reaction rates were calculated by the KMART6 module in the SCALE6.1 program.

2.3 Reactor optimization scheme

In our previous study, different fuel salt volume fractions (VF) and hexagon pitch sizes (P) were calculated and

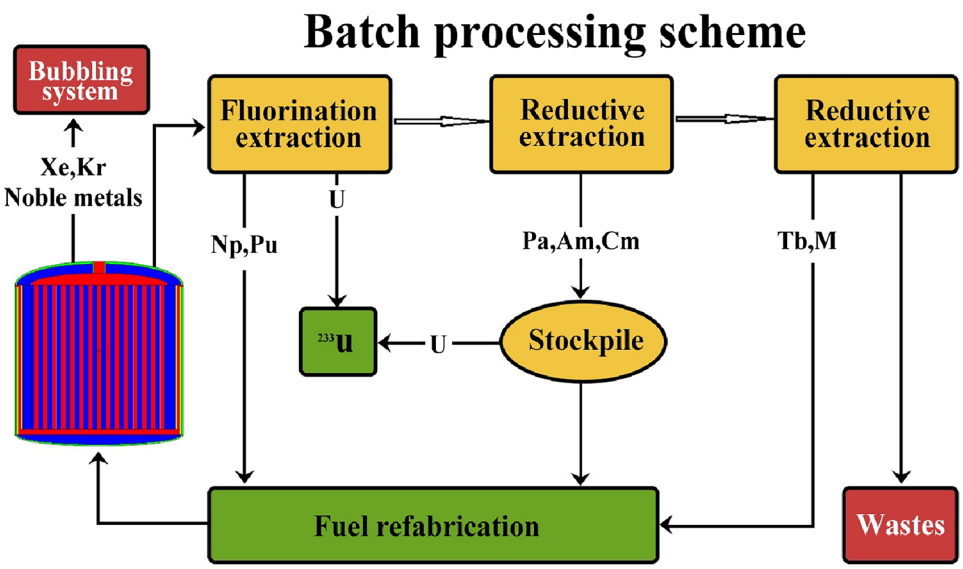

Fig. 2 Flowchart of reprocessing scheme

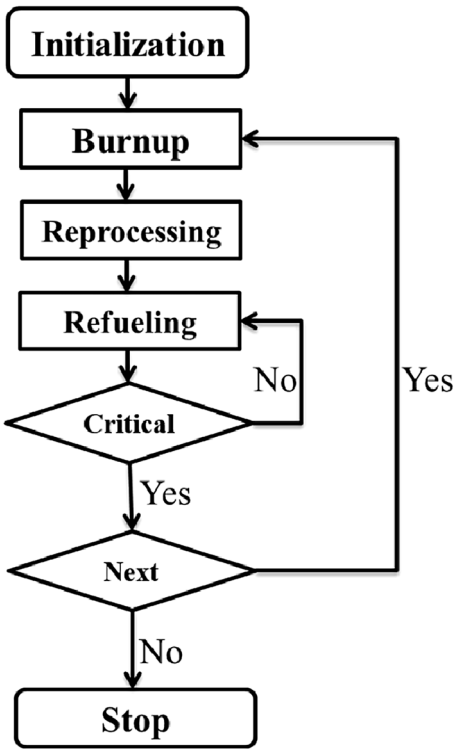

Fig. 3 Flowchart of calculation

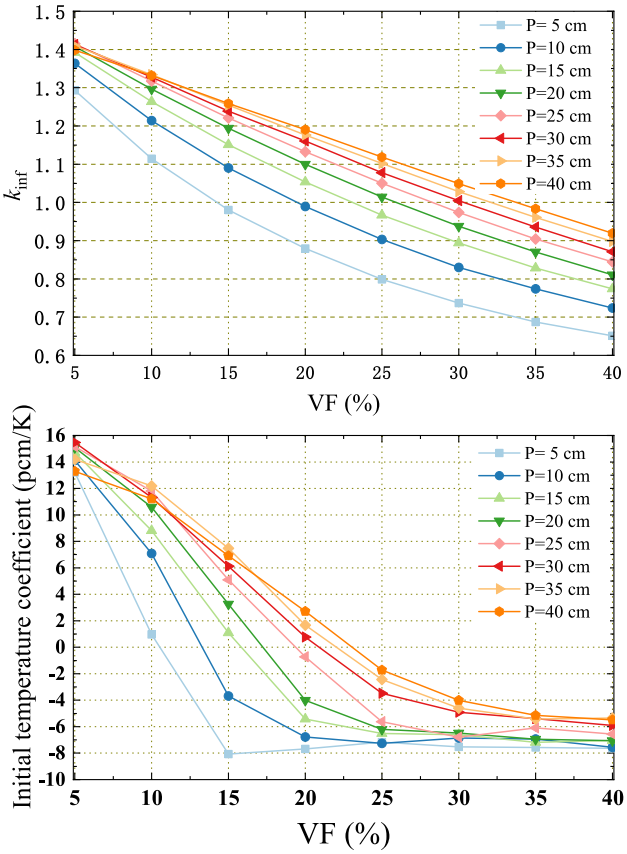

Fig. 4 (Color online) Time evolution of the initial k_{inf} and temperature reactivity coefficient for different volume fractions and pitch sizes

compared to evaluate their impact on the neutronics performance [31]. To obtain more specific results, the performance parameters of the ^{233}U production, plutonium utilization, MA accumulation, and passive safety for different volume fractions and pitch sizes were calculated to describe the burn-up performance in a small modular MSR.

The moderation ratio can be optimized by changing both the fuel channel radius and hexagon pitch size. The k_{inf} curve for different fuel volume fractions and pitch sizes is shown in Fig. 4. For larger fuel volume fraction values, the fission cross sections of ^{239}Pu and ^{241}Pu were smaller owing to significant hardening of the neutron spectrum. Therefore, within the research interval of this study, the value of k_{inf} was basically inversely proportional to volume fraction. In addition, the influence of the P size on k_{inf} cannot be underestimated. For larger P sizes, the neutron moderation was more inhomogeneous, thus the distribution of the neutron flux was relatively high in the low and high energy regions, and comparatively lower in the medium energy region. This form of the energy spectrum is more conducive to the fission reaction of plutonium and reduces the neutron resonance absorption, ultimately leading to a larger k_{inf}.

The evolution curve of the initial total temperature reactivity coefficient for different volume fractions and pitch sizes is also displayed in Fig. 4. The temperature coefficients dramatically decrease when volume fraction increases from 5% to 25%, from approximately 14 pcm/K to a negative value. The decrease in the temperature coefficient is influenced by the fuel doppler and graphite temperature effects.

The fuel doppler coefficient is negative within volume fraction values ranging from 10% to 25%. For a volume fraction value of less than 10%, the energy spectrum is softer, and broadening of the fission doppler of ^{239}Pu and ^{239}Pu caused by the increase in temperature is more apparent, thus the doppler coefficient becomes a positive value. For larger fuel volume fraction values, the energy spectrum becomes harder, the capture resonance contribution of other actinide nuclides is apparent, and the doppler coefficient becomes negative.

The coefficient of the graphite temperature rapidly decreases as the fuel volume fraction increases, and its variation depends on the competition between the capture reaction of ^{232}Th and the fission reaction of ^{239}Pu and ^{241}Pu. For smaller volume fraction values, the proportion of thermal neutrons is higher, and the increase of the graphite temperature causes the neutron energy spectrum to shift to ^{239}Pu and ^{239}Pu fission resonance peaks, resulting in an increased reactivity and positive graphite temperature coefficient. For larger volume fraction values, the neutron spectrum is

relatively hard and deviates from the fission resonance peaks of ^{239}Pu and ^{239}Pu. A higher graphite temperature is more favorable to the ^{232}Th capture reaction, resulting in a negative graphite reactivity coefficient.

The ^{233}U production, amount of TRUs, and MA accumulations for different fuel volume fractions ($P = 20$ cm) during the 50-year operation of the reactor is demonstrated in Fig. 5a, b, c, respectively. The comparative analysis results indicate that a higher thermal neutron flux is conducive to the incineration and utilization of plutonium, whereas a higher resonance neutron flux will deteriorate the neutronics performance. Although a higher fuel volume fraction can achieve a higher ^{233}U production, it will result in a higher capture fission ratio, lower neutron economy, and increased plutonium feed rates. Moreover, the accumulation of MAs increases as the fuel volume fraction increases, primarily owing to the higher initial plutonium loading and higher capture cross section of most of the actinide nuclides.

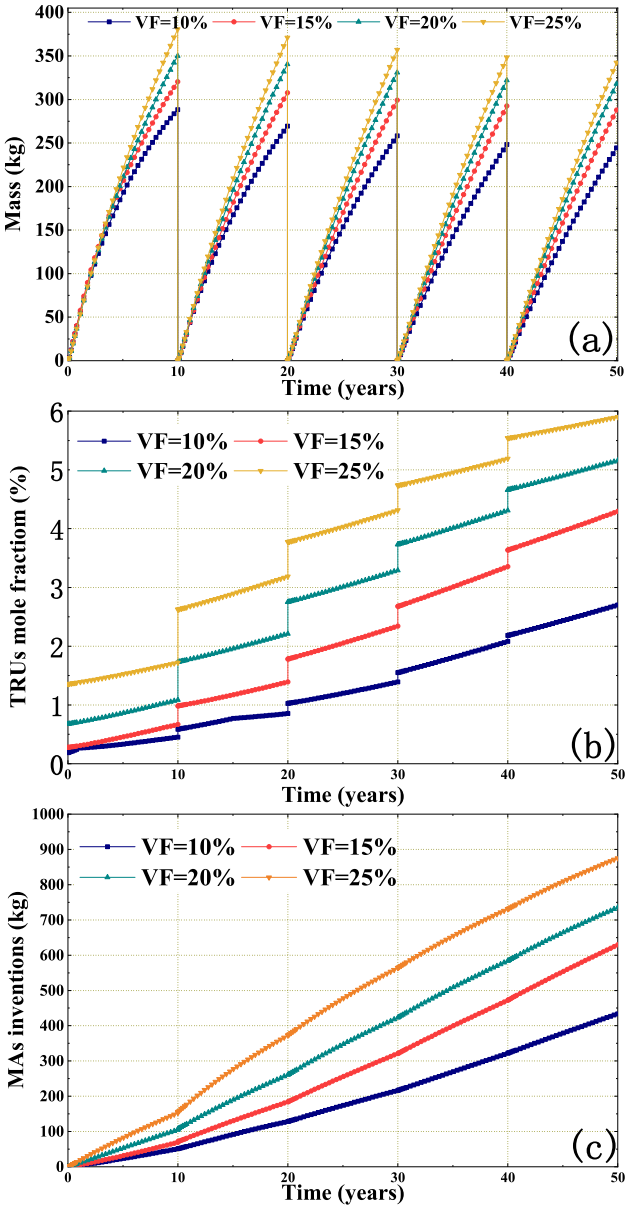

Fig. 5 (Color online) Time evolution of **a** ^{233}U productions, **b** amount of TRUs, and **c** MA accumulations for different volume fractions (when $P = 20$ cm)

In conclusion, within the research interval (VF=10% –40%, P=10 cm – 40 cm), a smaller volume fraction and larger P are preferable for a long-term operation and low radioactive residue, whereas a higher volume fraction and smaller P can contribute to the utilization of plutonium and production of ^{233}U. According to the aforementioned results, a smaller fuel volume fraction and higher P size are more favorable for improving the utilization efficiency of plutonium in a small MSR. After comprehensive consideration, a combination of $VF = 20\%$ and $P = 20$ cm was determined as a relatively excellent design parameter in this study.

3 Results and discussion

3.1 Neutron spectrum and flux

The performance of the burn-up process significantly depends on the neutron spectrum, which is largely determined by the core graphite moderation ratio. The normalized neutron energy spectra in various regions for the initial time, 10th year, and 50th year are displayed in Fig. 6, demonstrating that the neutron spectra in molten salt are slightly harder and those in the graphite reflector are the softest. In addition, as the running time increases, the spectra become harder, which occurs owing to the following: 1) increase in the reaction rate of the thermal neutron absorption owing to the accumulation of fission products; 2)buildup of plutonium loading and changes in the composition of the plutonium isotope. The absorption cross sections of ^{240}Pu and ^{242}Pu are significantly larger in the thermal neutron area and resonance energy region, and their mass fractions increase as the burnup time increases, which is critical for the hardening of the neutron spectrum.

The thermal power distribution is significantly impacted by the spatial distribution of the moderated neutron. The thermal neutron (< 0.625 eV) flux density for the entire reactor core decreases from the center to the edges; however, owing to the scattering effect of the graphite reflector, it slightly increases in the reflector. The maximum value of the thermal neutron flux density, with a peak value of approximately 1.128×10^{14}/ cm^2/s, was found near the geometric center of the active region, as shown in Fig. 7. The peak of the thermal neutron flux density was dispersed throughout the graphite assembly. The thermal neutron flux of the fuel channel exhibited an apparent declining peak, which was

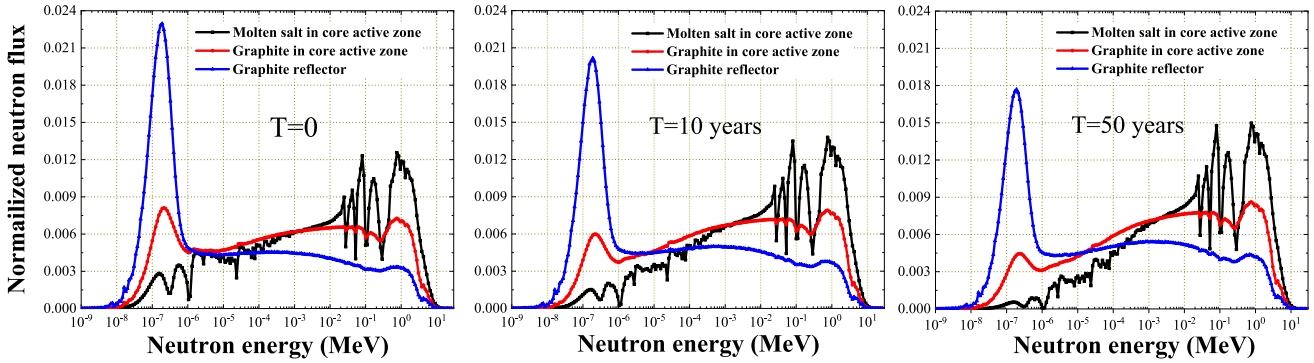

Fig. 6 (Color online) Normalized neutron energy spectra in different regions and at different operating times

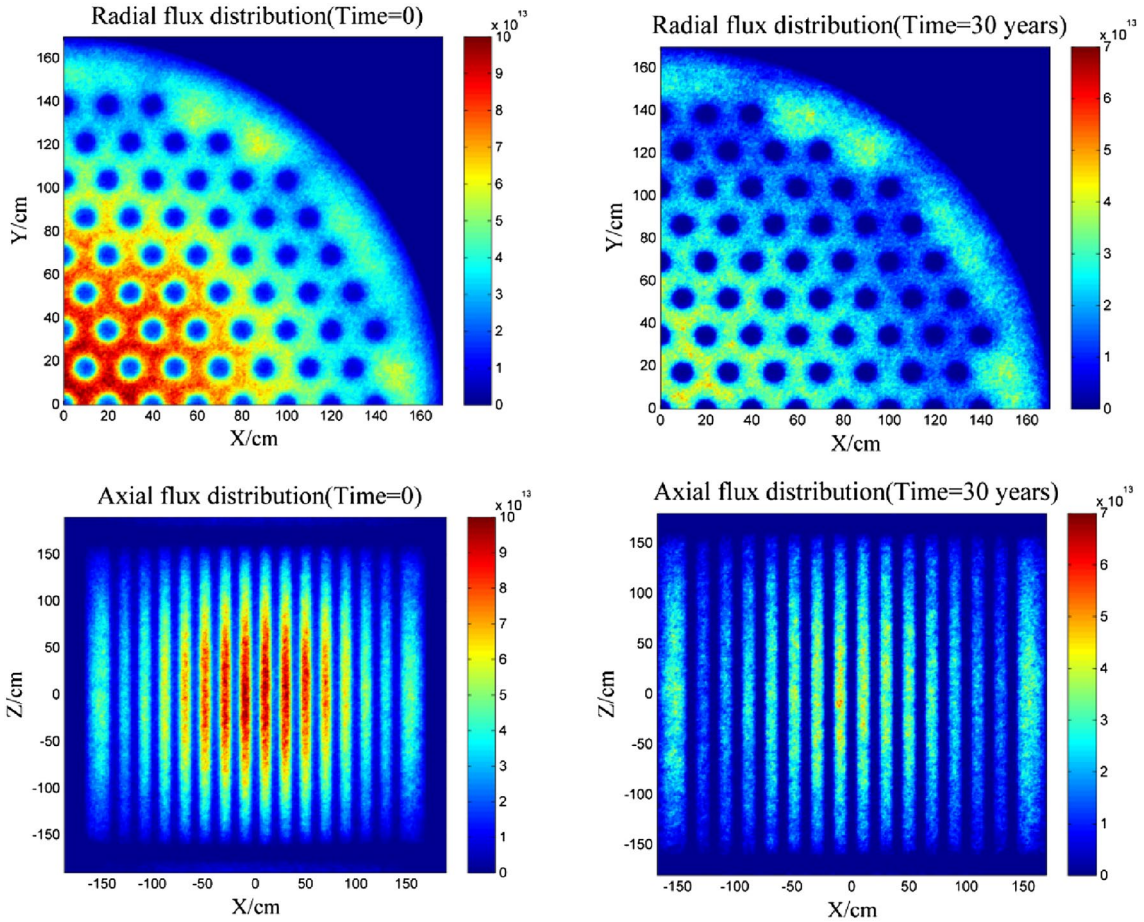

Fig. 7 (Color online) Spatial distribution of thermal neutron flux density

approximately 85% lower than that of the adjacent graphite. The total, axial, and radial peak power factors were 2.78, 1.75, and 1.70, respectively.

The lifespan of the graphite subassembly is significantly impacted by the spatial distribution of fast neutrons (>0.052 MeV); the distribution is complementarily symmetrical to that of the thermal neutron flux, demonstrating an apparent flux peak in the geometric center of the fuel salt channel, as shown in Fig. 8. Moreover, a larger diameter of the channel resulted in a higher flux peak. The geometric center of the active region also demonstrated the highest fast neutron flux density, which was approximately

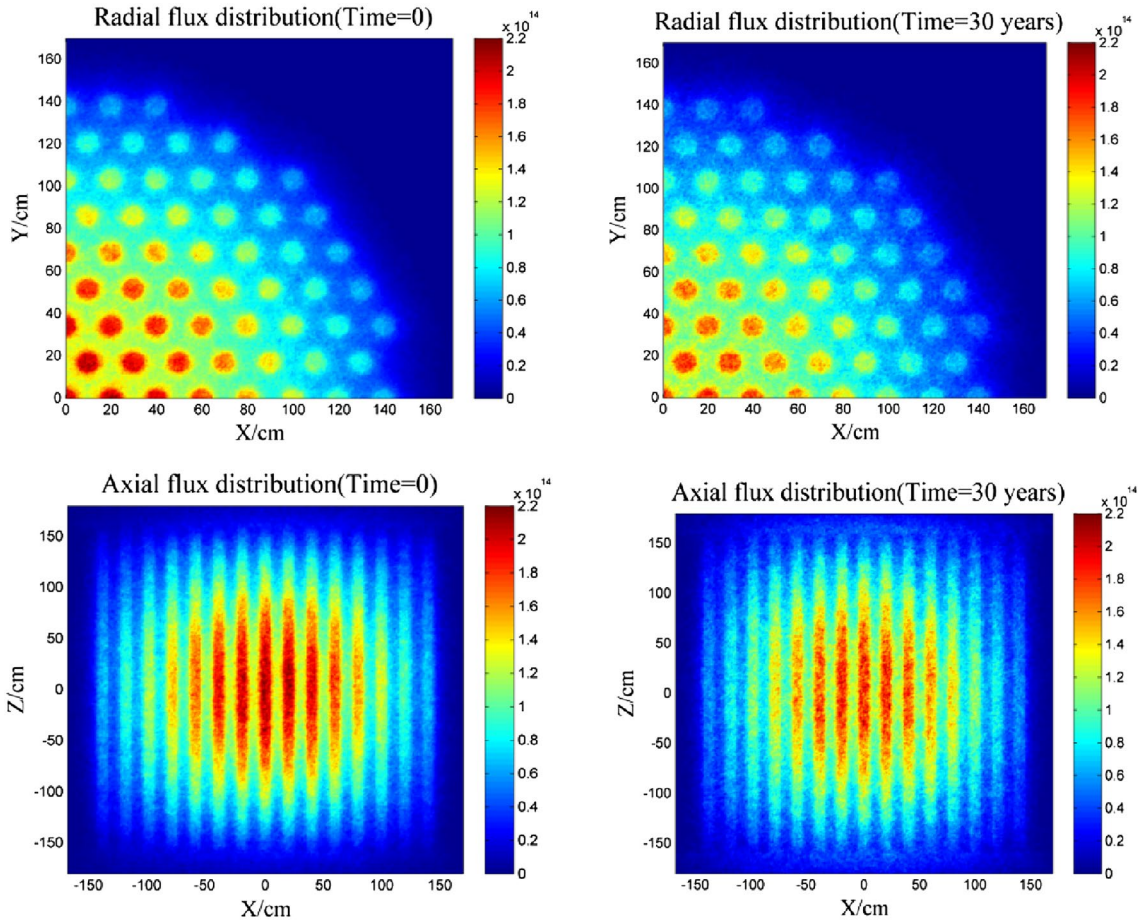

Fig. 8 Spatial distribution of fast neutron flux density

2.23×10^{14} / cm^2/s. The graphite reflector considerably lowered the fast neutron flux, which effectively reduced the radiation damage to the container vessel and extended its lifespan.

The average fast neutron flux density upon exposure to greater than 52 keV in the graphite assembly for the course of the first ten-year lifespan was determined to be approximately 1.04×10^{14} / cm^2/s. The lifespan of a graphite assembly is expected to be approximately 10 years based on the total fast neutron flux density that it can withstand (3×10^{22} / cm^2) [32, 33]. The graphite irradiation deformation may be significantly influenced by the wide gradient of the fast neutron flux from the channel wall to the center of the graphite assembly. The hexagonal graphite assembly has a large opposite side distance of 20 cm, which is good for fuel utilization and the temperature coefficient. However, further research is needed to determine the effect of the temperature distribution and irradiation stress on the life of the graphite assembly. The lifespan of the core of each generation of reactors may need to be reduced to eight, or shorter, if the graphite life does not satisfy the design criteria.

3.2 Amount of actinides and fission contribution

The fluctuations in the amount of primary actinides are complicated as a result of the periodic batch processing and continuous on-line fuel input while the system is in operation. Figure 9a presents the temporal evolution of the amount of actinide nuclides throughout the course of a five-generation reactor lifetime. Throughout the burn-up process, plutonium is continuously added to the fuel salts to compensate for the loss of reactivity, increasing the accumulation of plutonium in the core. Additionally, with each off-line fuel process, the accumulated uranium in the fuel salt is separated, and more plutonium is added to the fuel salt for starting the next-generation reactor, causing an increase in the accumulation of plutonium. MAs quickly accumulate to approximately one-tenth the amount of plutonium.

The total mass of thorium steadily decreases as the burn-up time increases. The loss of thorium is mostly used to absorb neutrons to form ^{233}Pa, which subsequently decays into ^{233}U. After each start-up, the amount of Pa quickly increases, tends to remain steady, and slightly decreases throughout the burn-up, primarily owing to the hardening

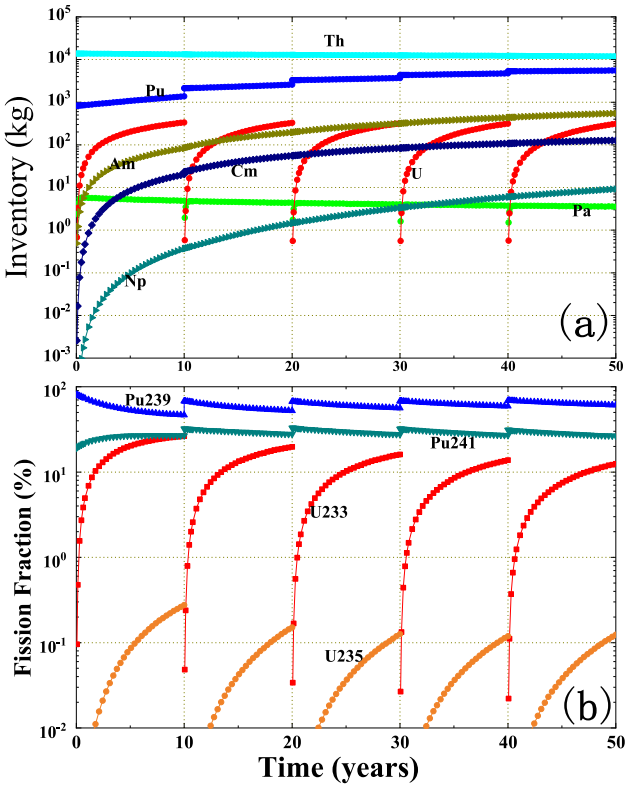

Fig. 9 (Color online) Evolution curves of the **a** amount of actinides and **b** the fission fraction for different fissile isotopes

of the energy spectrum and decrease in the ^{232}Th absorption reaction rate.

The fission cross section and fission contribution of plutonium decrease despite the amount of plutonium increasing, owing to the hardening of the energy spectrum. The amount of ^{233}U continues to increase throughout the course of the 10-year operation cycle, reaching approximately 300 kg before fuel-unloading, and the fission contribution of ^{233}U can surpass 10% at the end of each reactor-generation design life, as shown in Fig. 9b. The by-product content of ^{235}U is significantly low owing to the high purity of ^{233}U production, resulting in a significantly low fission fraction of ^{235}U, which is limited to 0.3%.

3.3 Net production and purity of ^{233}U

The production of ^{233}U, which is actually the accumulative total mass of ^{233}U mixed in the primary fuel salts, is significantly dependent on the neutron absorption of ^{232}Th. The reaction chain for the development of ^{232}Th into ^{233}U is expressed as follows:

$$^{232}\mathrm{Th} \xrightarrow{(n,\gamma)} {}^{233}\mathrm{Th} \xrightarrow{\beta} {}^{233}\mathrm{Pa} \xrightarrow{\beta} {}^{233}\mathrm{U}$$

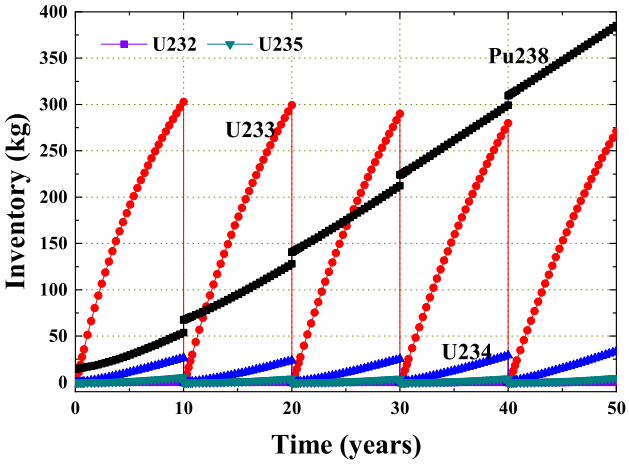

Fig. 10 (Color online)Time evolution of the amount of uranium isotopes

The total net ^{233}U production for a multi-generation operating cycle can be estimated by adding the amount of ^{233}U in the currently operating reactor and the product of (^{233}U + ^{233}Pa) extracted from the previous replaced core module. The real total production of ^{233}U can be calculated as follows:

$$^{233}\mathrm{U(Prod)} = {}^{233}\mathrm{U(Inv't)} + {}^{233}\mathrm{U(Ext)} + {}^{233}\mathrm{Pa(Ext)}, \quad (1)$$

where ^{233}U (Inv't) represents the residual ^{233}U mixed in the fuel currently in operation, ^{233}U (Ext) and ^{233}Pa (Ext) are the amounts of ^{233}U and ^{233}Pa extracted from the previously replaced core module.

Uranium is extracted from the fuel salt during each refueling cycle and stored outside the core, where it eventually becomes a high-purity ^{233}U product. Approximately 350 kg of uranium is produced and mixed in fuel salt during each 10-year operating cycle, as shown in Fig. 10. During the entire operating period, the increase in the accumulation of TRUs and hardening of the neutron spectrum will lead to a decrease in the ^{232}Th neutron absorption rate and ^{233}U annual production.

The purity of ^{233}U diminishes as the burn-up duration increases during each operating cycle. ^{238}Pu is continuously accumulated in fuel salts owing to the (n, 2n) reactions of ^{239}Pu. The α decay of ^{238}Pu produces ^{234}U, thus the increase in the amount of ^{238}Pu leads to an accumulation of ^{234}U, consequently decreasing the purity of ^{233}U. After 30 years of operation, the purity of ^{233}U can be maintained above 90%, which meets the demand for a pure thorium-uranium fuel cycle in a TMSR.

3.4 TRUs mole fraction and amount of MAs

The stability of the physical properties of the SM-MSR-Pu is restricted by the TRU mole fraction in fuel salt. The neutronics performance and physicochemical properties of fuel material are inevitably influenced by the build-up of TRUs. Every 10 days, approximately 5.8 kg of plutonium was loaded on-line into the fuel to compensate for the lost reactivity. Furthermore, approximately 700 kg of additional plutonium was added to the starting fuel for the next-generation reactor, leading to a significant increase in plutonium. The overall amount of plutonium accumulated increased from 821.61 kg to 5536 kg, despite 817.22 kg, 980.72 kg, 1015.83 kg, 1041.85 kg, and 1058.97 kg of plutonium being burned during the five fuel cycles. The time evolution of the amount of plutonium isotopes is shown in Fig. 11.

^{239}Pu and ^{239}Pu are the primary fissile materials and have relatively large fission cross sections. The amounts of ^{239}Pu and ^{239}Pu are typically stable over the period of each operational cycle of the generation-reactor, considering their consumption approximately equates to the amount of on-line feeding. The amount of ^{240}Pu demonstrated the fastest growth and surpassed that of ^{239}Pu within 50 years, which is mainly owing to the small capture cross-section and long alpha decay period (approximately 6594 y) of ^{240}Pu.

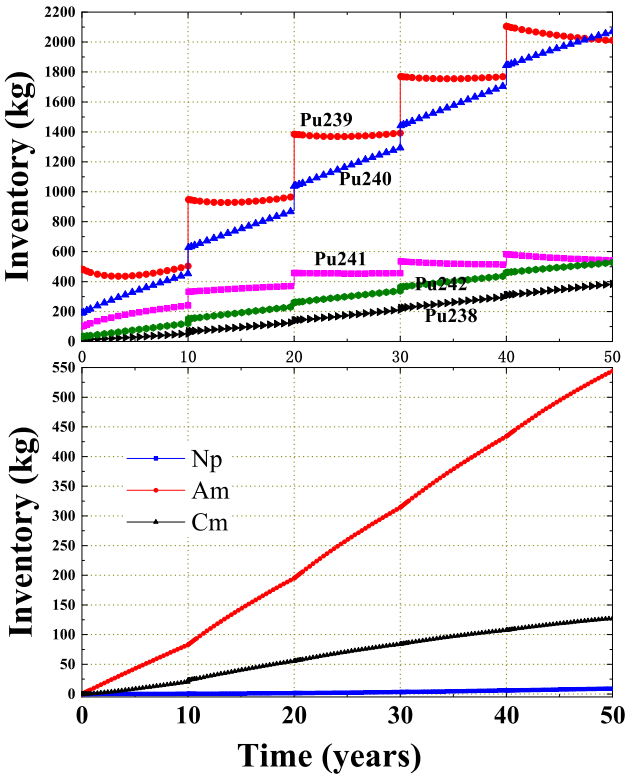

Fig. 11 (Color online) Amount of plutonium isotopes and MAs

The accumulated masses of MAs (primarily consisting of Np, Am, and Cm) reached 103.57 kg, 251.97 kg, 401.70 kg, 547.48 kg, and 680.92 kg within the five fuel cycles, respectively. The mass growth of Am was the fastest. The accumulation of ^{241}Am reached 409 kg, mainly owing to the beta decay of ^{239}Pu. The accumulation of ^{243}Am was also considerable (greater than 135 kg), which was mainly owing to the transformation of ^{242}Pu. Their nuclear chain reactions can be expressed as follows:

$$^{239}\mathrm{Pu} \xrightarrow{\beta(14.35y)} {}^{241}\mathrm{Am}$$

$$^{242}\mathrm{Pu} \xrightarrow{(n,\gamma)} {}^{243}\mathrm{Pu} \xrightarrow{\beta(4.956h)} {}^{243}\mathrm{Am}$$

The accumulation of Np is notably less than that of Am. The main sources of ^{237}Np are the α decay of ^{241}Am and β decay of ^{237}Np. Owing to the relatively long half-life period of ^{241}Am (approximately 432.2 years) and the four (n,γ) reactions required to convert ^{233}U to ^{237}Np, the production of ^{237}Np is constrained, and the accumulated mass of Np is the smallest. The chain reactions that produce ^{237}Np are as follows:

(1): $^{239}\mathrm{Pu} \xrightarrow{\beta(14.35y)} {}^{241}\mathrm{Am} \xrightarrow{(n,\alpha)} {}^{237}\mathrm{Np}$

(2): $^{233}\mathrm{U} \xrightarrow{(n,\gamma)} {}^{234}\mathrm{U} \xrightarrow{(n,\gamma)} {}^{235}\mathrm{U} \xrightarrow{(n,\gamma)} {}^{236}\mathrm{U} \xrightarrow{(n,\gamma)} {}^{237}\mathrm{Np} \xrightarrow{\beta(6.75d)} {}^{237}\mathrm{Np}$

To ensure the stability of the physical and chemical properties of fuel salts, the accumulation of TRU cannot exceed its upper solubility limit in molten salt. The mole fraction of the TRUs dramatically increased from the initial moment (7.6 times that of the initial fraction), as shown in Fig. 12. In the LiF-BeF_2 system, the solubility of PuF_3 mainly depends on the temperature of the carrier salt and the molar ratio of LiF and BeF_2, where the molar ratio is generally less than 1 mol% and the temperature ranges between 525–650 °C. However, adding UF_4 in the carrier salt will increase it by 2–3%. If FLiBe does not meet the requirements, the FLi carrier salt can be considered; the solubility of PuF_3 has

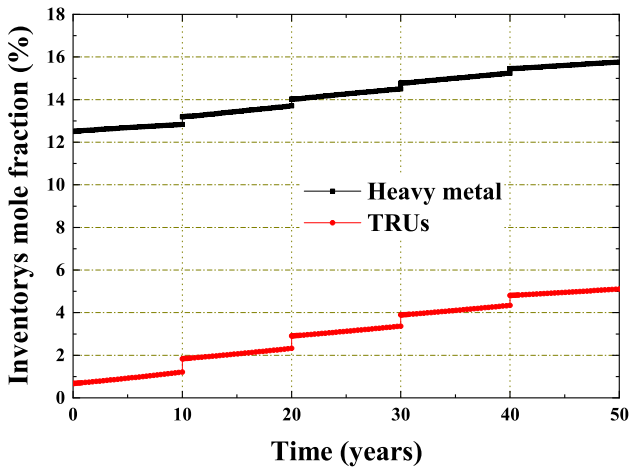

Fig. 12 (Color online) Mole fractions of the TRUs and total heavy metal

been improved, which is near 5 mol% in most temperature ranges. However, for the LiF-BeF_2 salt, the molar ratios of the TRUs increase to approximately 5% after 50 years of operation, exceeding the maximum solubility limit for TRUs. Therefore, a long-term operation of longer than 30 years may cause certain problems in the physical or chemical properties of the SM-MSR-Pu.

3.5 Temperature feedback coefficient and delayed neutron fraction

The temperature feedback coefficient is a critical factor for evaluating the passive safety performance. During the burn-up phase, the temperature coefficient must have a negative value to guarantee a safe operation of the reactor. The combined effects of the fuel doppler, fuel density, and graphite temperature determines the total temperature coefficient for the graphite-moderated molten salt reactors, as depicted in the following equation:

$$\left(\frac{\mathrm{d}\rho}{\mathrm{d}T}\right)_{\text{total}} = \left(\frac{\mathrm{d}\rho}{\mathrm{d}T}\right)_{\text{doppler}} + \left(\frac{\mathrm{d}\rho}{\mathrm{d}T}\right)_{\text{density}} + \left(\frac{\mathrm{d}\rho}{\mathrm{d}T}\right)_{\text{graphite}} \tag{2}$$

The over-time variations in the temperature reactivity coefficients are shown in Fig. 13, which clearly demonstrates that the coefficients of the graphite temperature and fuel doppler temperature are both negative and stable. The main contributing factor to the fuel doppler effect is the resonance absorption of actinides, particularly ^{240}Pu and ^{242}Pu. For fifty years, the temperature feedback coefficient owing to the fuel doppler effect is less than zero. The primary source of the graphite temperature coefficient is the modification of the energy spectrum owing to the increase in temperature. Within 50 years of the burn-up period, the graphite temperature coefficient fluctuates slightly between −2 and −3 pcm/K, which is relatively stable. The changing trend of the total temperature coefficient is highly influenced by the fuel density coefficient, which is primarily determined by the following two antagonistic factors: 1) As the temperature increases, the density of the molten salt decreases, and part of the fuel is forced out of the core, reducing the reactivity. 2) The decreased fuel salt density increases the volume ratio of the moderator, enhances the neutron moderation effect, and shifts the neutron spectrum towards the thermal zone, resulting in an increase in the reactivity. Owing to the latter effect being more pronounced among the two, the density coefficient is positive most of the time, as shown in Fig. 13. During a long-term operation, the increase in plutonium will increase the first effect, which is beneficial for a negative coefficient of the total temperature reaction.

The effective delayed neutron fraction (DNF) is shown in Fig. 14. The initial effective DNF, which is 280 pcm in the absence of a fuel flow, is mostly contributed by ^{239}Pu. At the end of the initial 10-year operational period, the effective DNF increased to 325 pcm owing to the accumulation of ^{239}Pu.

For the actual operation of the MSR, the fuel salt flow will reduce the DNF in the core. The effective DNF under a stationary flow can be defined by the point kinetics equations as follows [34]:

$$\beta_{\text{i,flow}} = \beta_{\text{i,static}} \frac{\lambda_{\text{i}}}{\lambda_{\text{i}} + \frac{1}{\tau_{\text{c}}}\left(1 - \exp\left(-\lambda_{\text{i}}\tau_{\text{L}}\right)\right)} \tag{3}$$

The residence time inside the reactor core is denoted by τ_{c}, whereas τ_{L} is the residence time outside the reactor core. For most operating conditions of the SM-MSR-Pu, the flow effect can reduce the reactivity by more than 100 pcm. The

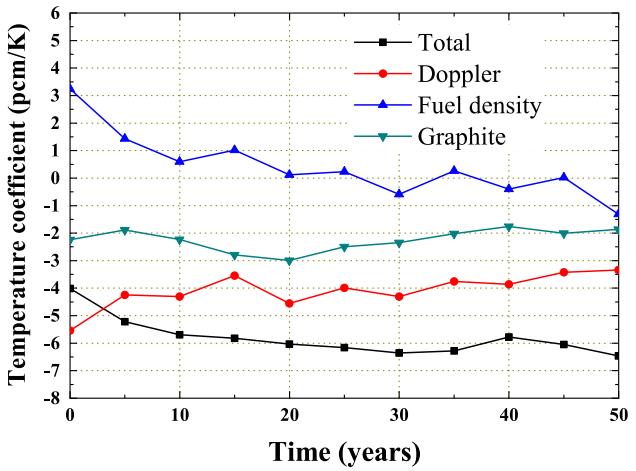

Fig. 13 (Color online) Evolution of the temperature reactivity coefficient

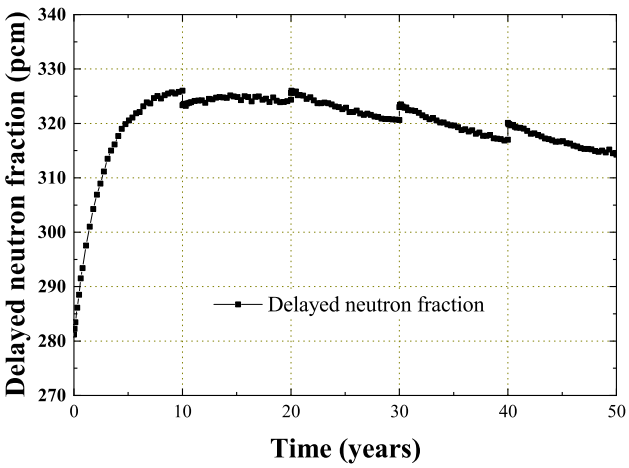

Fig. 14 Evolution of delayed neutron fraction

reactivity loss is more sensitive to the residence time inside the active core, and notably increases at the lower residence times. The fuel salt flow velocity and volume distribution determine the residence time; therefore, variations in the flow velocity during the transition process may result in a change in the residence time. A higher flow velocity results in a shorter residence time, thus the loss of reactivity is approximately proportional to the velocity. The instantaneous shutdown of the primary pump may introduce a positive reactivity of approximately 100 pcm, which should be considered particularly for the design and operation of molten salt reactors.

To provide a design margin for the passive safety, thermal disturbance, and reactivity control, the total temperature reactivity coefficient of the SM-MSR-Pu is required to be less than −3.5 pcm/K. For the SM-MSR-Pu, the temperature feedback coefficient is consistently negative and exhibits a downward trend, which ensures a long-term safe operation. Detailed data are shown in Table 2.

3.6 Fuel utilization and optimization Schemes

An overview of the consumption and production of certain actinide components is presented in Table 3, in which the initial loading, on-line feeding, quantity, and net production or consumption are counted. For the 50-year operation, 1882.2 kg of thorium and 4890 kg of plutonium was consumed, and 1443.2 kg of ^{233}U was newly produced. The mass of uranium quickly reached 350 kg over each 10-year refueling cycle, and the purity of ^{233}U was at least 90%. The annual production capacity of ^{233}U per the unit thermal power for five generations of reactors was 0.121, 0.120, 0.116, 0.112, and 0.108 kg/y/MWt, respectively. However, after the five generations of the reactor, there was an accumulation of approximately 9.173 kg Np, 544.36 kg Am, and 127.39 kg Cm in the fuel salt.

The stability of the physical and chemical properties of the SM-MSR-Pu may have certain issues with a long-term operation. First, the annual production and purity of ^{233}U both decrease during the five-generations of the reactor operation. Second, the rapid accumulation of MAs will increase the difficulty of reprocessing radioactive spent fuel. Lastly, and most importantly, the accumulated mass of TRU may exceed the solubility limit of the FLiBe salt owing to the increasing amount of the plutonium and MAs. Therefore, for a long-term stable functioning of SM-MSR-Pu and for a more effective utilization of the plutonium resource, further research is suggested, for which two feasible optimization schemes are provided herein. Scheme I proposes to extract and separate MAs. The MAs that have accumulated in the core of the 3rd operation cycle will be removed and geologically buried, instead of being transferred back to the core of the 4th operation cycle. The amount of plutonium and the molar fraction of TRUs can both be significantly reduced with this strategy while increasing the accumulation of MAs. Scheme II suggests reducing on-line plutonium feeding as follows: beginning with the 4th operation cycle, no additional plutonium will be supplied to the core to compensate for the reactivity loss. As an alternative, ^{233}U produced in the previous generation of reactors will be added on-line to the core as a fissile fuel. This method has the potential to transition to a pure thorium-uranium fuel cycle and minimize the increment of MAs, albeit at the expense of reducing ^{233}U production.

Table 2 Temperature reactivity coefficients for five operation cycles

Operation cycle	G1		G2		G3		G4		G5	
Time (years)	0	10	0	10	0	10	0	10	0	10
Total	−4.01	−5.69	−6.57	−6.03	−6.31	−6.35	−6.03	−5.78	−7.38	−6.46
Doppler	−5.54	−4.30	−4.71	−4.55	−3.86	−4.31	−3.44	3.86	−3.71	−3.34
Density	3.24	0.59	1.86	0.12	0.79	−0.59	−0.10	−0.40	−0.38	−1.31
Graphite	−2.24	−2.24	−3.37	−2.99	−2.73	−2.35	−3.33	−1.76	−2.56	−1.86

Table 3 Fuel balance for 30 years and 50 years operation

Operation cycle	Operation time = 30 years				Operation time = 50 years			
Isotopes	^{232}Th	^{233}U	Pu	MAs	^{232}Th	^{233}U	Pu	MAs
Initial loading (kg)	13829.2	0	821.6	0	13829.2	0	821.6	0
On-line feeding (kg)	0	0	5718.1	0	0	0	9604.9	0
Extraction(kg)	0	602.2	0	0	0	1172.1	0	0
Amount (kg)	12580.0	290.0	3692.3	401.7	11940.0	271.1	5536.5	680.9
Net changes(kg)per decade	−416.4	+297.4	−949.1	+133.9	−377.84	+288.64	−978.0	+136.2

4 Conclusion

The SM-MSR-Pu based on off-line batch processing that utilizes plutonium as the starting fuel was developed to achieve the efficient utilization of PWR spent fuel and thorium resources. The structural design and fuel management scheme of the SM-MSR-Pu were presented. Batch fuel reprocessing, plutonium incineration, and ^{233}U production are the primary factors considered in the design of SM-MSR-Pu.

The neutron energy spectrum, spatial distribution of the neutron flux, and temperature reactivity coefficient were calculated to analyze the neutronics properties, graphite irradiation life, and safety performance. The lifespan of a graphite assembly was calculated to be approximately 10 years. However, the effects of the temperature distribution and irradiation stress on the lifespan of the graphite assembly require further investigation. If the graphite life does not meet the design requirements, it is critical to modify the power density or shorten the replacement time of the container. The temperature feedback coefficient was consistently negative and decreased from −4.0 pcm K^{-1} to −6.5 pcm K^{-1} over the 50-year operating time, which guarantees a safe long-term operation.

The production and purity of ^{233}U, consumption and amount of plutonium, and accumulation of MAs were presented to analyze the fuel burn-up performance of the SM-MSR-Pu. The results indicate that Plutonium is a feasible and advantageous starting fuel for a SM-MSR, but presents certain shortcomings that need to be solved. Based on the specific design and fuel management solutions, SM-MSR-Pu can reduce the dependence of nuclear reactors on uranium resources by efficiently burning plutonium extracted from pressurized water reactors. The SM-MSR-Pu demonstrated that approximately 288.64 kg ^{233}U can be produced while 978.00 kg of plutonium is burned every decade, and the purity of ^{233}U was greater than 90%. Note, as the running time increases, the annual production and purity of ^{233}U will decrease, the amount of plutonium and accumulation of the MAs will increase, and the molar fraction of TRU may exceed the solubility limit. To achieve an optimal burn-up performance, setting the entire operation time to 30 years is advisable. However, 2847.3 kg of plutonium was consumed and more than 3600 kg of plutonium will eventually accumulate in the core. Further utilization of this accumulated plutonium will be a significantly complex problem.

To ensure the long-term stable operation of SM-MSR-Pu and more efficiently utilize plutonium, more physical features of the SM-MSR-Pu must be further investigated, and two feasible optimization schemes are provided in Sect. 3.6 for the reference of future research.

Author Contributions All authors contributed to the study conception and design. Material preparation, data collection, and analysis were performed by Xue-Chao Zhao, Rui Yan, and Yang Zou. The first draft of the manuscript was written by Xue-Chao Zhao, and all authors commented on previous versions of the manuscript. All authors read and approved the final manuscript.

Data Availability Statement The data that support the findings of this study are openly available in Science Data Bank at https://cstr.cn/31253.11.sciencedb.16182 and https://doi.org/10.57760/sciencedb.16182.

Declarations

Conflict of interest Xiang-Zhou Cai is an editorial board member for Nuclear Science and Techniques and was not involved in the editorial review, or the decision to publish this article. All authors declare that there are no Conflict of interest.

References

1. U.S. Doe, A technology roadmap for generation four nuclear energy systems. Philos. Rev. **66**, 139–241 (2002)
2. R.C. Robertson. Conceptual design study of a single-fluid molten-salt breeder reactor. comp. Oak Ridge National Lab. Tenn. (1971). https://doi.org/10.2172/4030941
3. M.W. Rosenthal, P.R. Kasten, R.B. Briggs, Molten-salt reactors-history, status, and potential. Nuclear Technol. **8**, 107–117 (1970)
4. J. Křepel, B. Hombourger, C. Fiorina et al., Fuel cycle advantages and dynamics features of liquid fueled MSR. Ann. Nucl. Energy. **64**, 380–397 (2014). https://doi.org/10.1016/j.anucene.2013.08.007
5. G.C. Li, Y. Zou, C.G. Yu et al., Influences of ^{7}Li enrichment on Th-U fuel breeding for an improved molten salt fast reactor (IMSFR). Nucl. Sci. Tech. **28**, 97–105 (2017). https://doi.org/10.1007/s41365-017-0250-7
6. A. Nuttin, D. Heuer, A. Billebaud et al., Potential of thorium molten salt reactors detailed calculations and concept evolution with a view to large scale energy production. Prog. Nucl. Energy. **46**, 77–99 (2005). https://doi.org/10.1016/j.pnucene.2004.11.001
7. D. LeBlanc, Molten salt reactors: a new beginning for an old idea. Nucl. Eng. Des. **240**, 1644–1656 (2010). https://doi.org/10.1016/j.nucengdes.2009.12.033
8. M.S. Cheng, Z.M. Dai, Development of a three dimension multi-physics code for molten salt fast reactor. Nucl, Sci. Tech. **25**, 10601 (2014). https://doi.org/10.13538/j.1001-8042/nst.25.010601
9. M. Brovchenko, J.L. Kloosterman, L. Luzzi et al., Neutronic benchmark of the molten salt fast reactor in the frame of the EVOL and MARS collaborative projects. EPJ Nuclear Sci. Technol. **5**, 2 (2019)
10. P.N. Haubenreich, J.R. Engel, Experience with the molten salt reactor experiment. Nucl. Appl. Tech. **8**, 118–136 (1970)
11. W.B. Cottrell, H.E. Hungerford, J.K. Leslie et al., Operation of the aircraft reactor experiment. No. ORNL-1845 (Del.). Oak Ridge National Lab. Tenn. (1955). https://doi.org/10.2172/4237975
12. X.C. Zhao, D.Y. Cui, X.Z. Cai et al., Analysis of Th-U breeding capability for an accelerator-driven subcritical molten salt reactor. Nucl. Sci. Tech. **29**, 121 (2018). https://doi.org/10.1007/s41365-018-0448-3
13. L.Y. He, S.P. Xia, X.M. Zhou et al., Conceptual design and neutronic analysis of a megawatt-level vehicular micro reactor

based on TRISO fuel particles and S-CO2 direct power generation. Nucl. Sci. Tech. **33**, 69 (2022). https://doi.org/10.1007/s41365-022-01064-4
14. F.Y. Zhang, G.F. Zhu, Y. Zou et al., Application of Monte Carlo method to calculate the effective delayed neutron fraction in molten salt reactor. Nucl. Sci. Tech. **30**, 34 (2019). https://doi.org/10.1007/s41365-019-0557-7
15. C.Y. Zou, J.H. Wu, C.G. Yu et al., Influence of reprocessing efficiency on fuel cycle performances for molten salt reactor. Nucl. Tech. **44**, 48–54 (2021). https://doi.org/10.11889/j.0253-3219.2021.hjs.44
16. M. Kutt, F. Friederike, M. Englert, Plutonium disposition in the BN-800 fast reactor. Sci. Glob. Secur. **22**, 188–208 (2014). http://doi.org/10.1080/08929882.2014.952578
17. E. Merle-Lucotte, D. Heuer, C.Le. Brun et al., Fast thorium molten salt reactors started with plutonium. Proceedings of ICAPP'06. American Nuclear Society, 6132-9 (2006)
18. D.Y. Cui, S.P. Xia, X.X. Li et al., Transition towards thorium fuel cycle in a molten salt reactor by using plutonium. Nucl. Sci. Tech. **28**, 152 (2017). https://doi.org/10.1007/s41365-017-0303-y
19. D.T. Ingersoll, Deliberately small reactors and the second nuclear era. Prog. Nucl. Energy. **51**, 589–603 (2009). https://doi.org/10.1016/j.pnucene.2009.01.003.8
20. P. Sabharwall, E. Kim, M. Mckellar et al., Small Modular Molten Salt Reactor (SM-MSR). In: ASME 2011 Small Modular Reactors Symposium, 31–39 (2011). https://doi.org/10.1115/SMR2011-6527
21. Y.W. Ma, J.G. Chen, X.Z. Cai et al., Preliminary quantitative proliferation resistance assessment of small modular thorium based MSR. Atom. Energy Sci. Technol. **52**, 1994–2000 (2018). https://doi.org/10.7538/yzk.2018.youxian.0162
22. K. Mitachi, T. Yamamoto, R. Yoshioka, Self-sustaining core design for 200 MWe molten-salt reactor with thorium-uranium fuel: FUJI-U3-(0). In: Proceedings of TU2007,4-6(2007)
23. J.C. Mailen, G.I. Cather Fluorination of falling droplets of molten fluoride salt as a means of recovering uranium and plutonium. ORNL-4224, 1980. https://doi.org/10.2172/4835210
24. K. Mitachi, Y. Yamana, T. Suzuki et al., Neutronic examination on plutonium transmutation by a small molten-salt fission power station. No.IAEA-TECDOC–840.1995
25. B.R. Betzler, J.J. Powers, A. Worrall et al.,Two dimensional neutronic and fuel cycle analysis of the transatomic power molten salt reactor. Office of Scientific and Technical Information (OSTI), ORNL/TM- 2016/742.(2017).https://doi.org/10.2172/1340461
26. C.Y. Zou, X.Z. Cai, C.G. Yu et al., Transition to thorium fuel cycle for TMSR. Nucl. Eng. Des. **330**, 420–428 (2018). https://doi.org/10.1016/j.nucengdes.2018.01.033
27. C.Y. Zou, X.Z. Cai, D.Z. Jiang et al., Optimization of temperature coefficient and breeding ratio for a graphite moderated molten salt reactor. Nucl. Eng. Des. **281**, 114–120 (2015). https://doi.org/10.1016/j. nucengdes.2014.11.022
28. G.C. Li, P. Cong, C.G. Yu et al., Optimization of Th-U fuel breeding based on a single-fluid double-zone thorium molten salt reactor. Prog. Nucl. Energy. **108**, 144–151 (2018). https://doi.org/10.1016/j.pnucene.2018.04.017
29. D. Heuer, E. Merle-Lucotte, M. Allibert et al., Towards the thorium fuel cycle with molten salt fast reactors. Ann. Nucl. Energy **64**, 421–429 (2014). https://doi.org/10.1016/j.anucene.2013.08.002
30. C.G. Yu, C.Y. Zou, J.H. Wu et al., Development and verification of molten salt reactor refueling and reprocessing system analysis code based on SCALE. Atom. Energy Sci. Technol. **52**, 12 (2018). http://dx.doi.org/10.7538/yzk.2018.youxian.0123 **(in Chinese)**
31. X.C. Zhao, Y. Zou, R. Yan et al., Analysis of burnup performance and temperature coefficient for a small modular molten-salt reactor started with plutonium. Nucl. Sci. Tech. **34**, 17 (2023). https://doi.org/10.1007/s41365-022-01155-2
32. J.R. Engel, H.F. Bauman, J.F. Dearing et al., *Conceptual design characteristics of a denatured molten-salt reactor with once through fueling* (Oak Ridge National Lab, TN, USA, 1980)
33. K. Nagy, J.L. Kloosterman, D. Lathouwers et al., The effects of core zoning on the graphite lifespan and breeding gain of a moderated molten salt reactor. Ann. Nucl. Energy. **43**, 19–25 (2012). https://doi.org/10.1016/j.anucene.2011.12.025
34. G.F. Zhu, R. Yan, H.H. Peng et al., Application of Monte Carlo method to calculate the effective delayed neutron fraction in molten salt reactor. Nucl. Sci. Tech. **30**, 34 (2019). https://doi.org/10.1007/s41365-019-0557-7